JVST B
Journal of Vacuum Science & Technology B

Shape and dose control for proximity effect correction on massively parallel electron-beam systems

Cite as: J. Vac. Sci. Technol. B **38**, 062603 (2020); https://doi.org/10.1116/6.0000556
Submitted: 15 August 2020 • Accepted: 07 October 2020 • Published Online: 29 October 2020

Md Nabid Hasan, Soo-Young Lee, Byung-Sup Ahn, et al.

JVST B
Journal of Vacuum Science & Technology B

ARTICLE

avs.scitation.org/journal/jvb

Shape and dose control for proximity effect correction on massively parallel electron-beam systems

Cite as: J. Vac. Sci. Technol. B 38, 062603 (2020); doi: 10.1116/6.0000556
Submitted: 15 August 2020 · Accepted: 7 October 2020 ·
Published Online: 29 October 2020

Md Nabid Hasan,[1] Soo-Young Lee,[1,a)] Byung-Sup Ahn,[2] Jin Choi,[2] and Joon-Soo Park[2]

AFFILIATIONS

[1]Department of Electrical and Computer Engineering, Auburn University, Auburn, Alabama 36849
[2]Samsung Electronics, Mask Development Team, 16 Banwol-Dong, Hwasung, Kyunggi-Do 18448, South Korea

Note: This paper is part of the collection: Electron, Ion, and Photon Beam Technology and Nanofabrication, EIPBN 2020.
[a)]**Electronic mail:** leesooy@eng.auburn.edu

ABSTRACT

Massively parallel electron-beam (e-beam) systems (MPESs) were developed to increase the writing throughput and demonstrated to be able to write large-scale patterns significantly faster compared to conventional single-beam systems. However, such systems still suffer from the inherent proximity effect due to the electron scattering in the resist. The proximity effect correction (PEC) has been investigated for a long time, and several PEC schemes have been proposed. Though most of the PEC schemes may be employed for an MPES, their direct application would be subject to the system's constraints, e.g., a relatively large beam size, a fixed exposing interval, and the same deflection angle for all beams, which may lead to nonoptimal correction results. In this work, practical methods for realizing various types of spatial dose distributions required for the PEC and implementing both shape and dose corrections under the MPES constraints have been developed. It has been shown that, with these methods, the proximity effect correction can be performed effectively with the critical dimension error, line edge roughness, and total dose taken into account.

I. INTRODUCTION

One of the major limiting factors in electron-beam (e-beam) lithography (EBL) is the geometric distortion of written features due to electron scattering, i.e., the proximity effect, which limits the minimum feature size and the maximum circuit density that can be achieved. The importance of the proximity effect correction (PEC) has been well recognized and extensively investigated, and various effective schemes have been developed to improve the accuracy of critical dimension (CD).[1–6] Another problem to consider is the line edge roughness (LER), which is caused by a number of stochastically fluctuating effects such as shot noise, distributions of chemical species in the resist, resist development process, etc.[7] Since the LER does not scale with the feature size, it can significantly limit the minimum feature size and maximum circuit density that can be realized. Therefore, it is necessary to minimize the LER in order to be able to continue enhancing the feature resolution and pattern density that can be achieved by the EBL. Also, it is often desired to minimize the total dose because a lower total dose reduces the e-beam writing time and the charging effect.

A typical approach to the PEC employs one of the dose, shape, and shape + dose corrections. In a single-beam e-beam system, whether a Gaussian or variable-shape beam, the beam size on the resist surface is or can be made small (∼1 nm) so that a sufficient spatial resolution can be achieved in both shape and dose corrections. On the other hand, in the massively parallel e-beam system (MPES), e.g., the eMET,[8] MBM-1000,[9] and MAPPER Lithography FLX-1200 tool,[10] the beam size is relatively large (∼10 nm), and the exposing interval is fixed, usually the same as the beam size. Therefore, the adjustment of feature size for the shape correction and the spatial modulation of dose for the dose correction can be limited, leading to a nonoptimal correction result, unless the optimal reduction (ΔW) of linewidth is an integer multiple of the beam size. Therefore, an effective method enabling an adjustment of feature size and a spatial dose modulation at the resolution of sub-beam-size is required.

In a previous study,[6] four different spatial dose distributions were considered for the PEC, i.e., uniform, V-type, A-type, and M-type. It was shown that the A-type distribution is effective when the aspect ratio (resist thickness to feature width) is relatively large while the uniform or V-type distribution tends to work better for a relatively small aspect ratio. Also, in another study,[7] it was observed that when the edge location of a developed feature is outside the exposed area, the LER tends to be small compared to that when the edge location is inside the exposed area. In this study, a systematic method for realizing various types of spatial dose distributions with an arbitrary reduction of feature size on an MPES is developed. The method utilizes the multipass writing, i.e., exposes each writing path multiple times, in realizing a spatial dose distribution. Also, an effective method of PEC utilizing both shape and dose corrections with spatial dose distributions realizable on an MPES is designed. The results show that when the reduction of feature size is not an integer multiple of the beam size, smaller CD error and LER are achieved in most cases, which well justifies the need for and effectiveness of the proposed methods. In this paper, the detailed description of the methods and the results from an extensive simulation are provided.

The rest of the paper is organized as follows. The simulation model is depicted in Sec. II. In Sec. III, the realization of uniform, V-type, A-type, and M-type dose distributions for different ΔW are described. The shape + dose correction algorithm for minimizing the CD error and LER is described in Sec. IV. Simulation results are discussed in Sec. V, followed by a summary in Sec. VI.

II. MODEL

A model of MPES is employed in this simulation study, which is derived from the eMET[8] and MBM-1000,[9] where beams are arranged in a 2D array of 512×512, the cross section of a beam is a square of $10 \times 10\,\text{nm}^2$, and the beam energy is 50 KeV. Each beam can be turned on or off individually, and beams are deflected in a synchronized manner, i.e., the same angle and direction. In this section, the exposure process in the MPES is described along with the coordinate and substrate systems, and the modeling of the transfer function (TF) is explained.

A. Exposure process

It is assumed in this study that the resist layer of a substrate system is on the X-Y plane, and parallel beams are in the Z direction, i.e., normal to the X-Y plane, as illustrated in Fig. 1. The resist layer to be exposed can be modeled as an array of square-shaped pixels with size $B \times B$, the same as the beam size on the resist (Fig. 1). Rows and columns of pixels or beams are in the X and Y dimensions, respectively. The exposing interval, I_{ex}, can be larger, smaller, or equal to B. For simplicity, it is assumed that $I_{ex} = B$ throughout this paper.

The 3D transfer function is denoted by $TF(x, y, z)$, describing the exposure distribution in the resist when a point (pixel) is exposed by a beam. Then, the 3D spatial distribution of exposure,

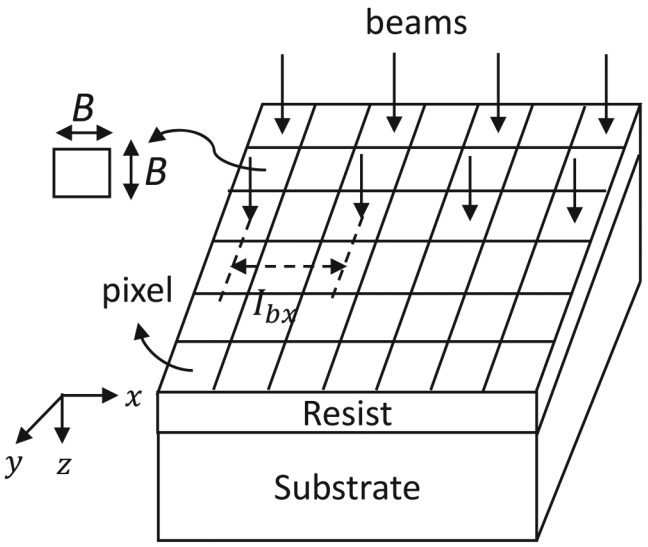

FIG. 1. Coordinate system employed in this study. The substrate moves in the X direction exposed by parallel beams: the beam size is $B \times B$, and the beam interval is I_{bx}.

$E(x, y, z)$, can be expressed by the following convolution:

$$E(x, y, z) = \int_{y'} \int_{x'} d(x - x', y - y') TF(x', y', z)\, dx'\, dy', \quad (1)$$

where $d(x, y)$ represents the dose distribution given by all beams.

B. Transfer function

An ideal TF may be defined to be constant within the area of $B \times B$ and zero outside for all layers of resist. However, a real TF deviates from the ideal one due to the beam blur and the electron scattering in the resist layers (Fig. 2).[9] The TF is modeled by the convolution of the ideal TF and a Gaussian function.[11] The standard deviation σ_t of the Gaussian function, to be referred to as *blurring factor*, quantifies the level of beam blur and electron scattering. A smaller σ_t results in a transfer function closer to the ideal one and leads to a lower level of proximity effect.

The CD of a feature, estimated based on the stochastic exposure, can be larger than the CD based on the deterministic exposure.[12] Since the exposure in the resist is inherently stochastic, a stochastic model of transfer function is necessary to obtain realistic results. A certain percentage of Gaussian noise is added to the (deterministic) transfer function, $TF_d(x, y, z)$, to model the stochastic exposure as follows:

$$TF_s(x, y, z) = TF_d(x, y, z) + TF_n(x, y, z), \quad (2)$$

$$TF_n(x, y, z) = c\epsilon TF_d(x, y, z) \left(\frac{TF_d(x, y, z)}{\max_{x,y} (TF_d(x, y, z))} \right)^{\alpha}, \quad (3)$$

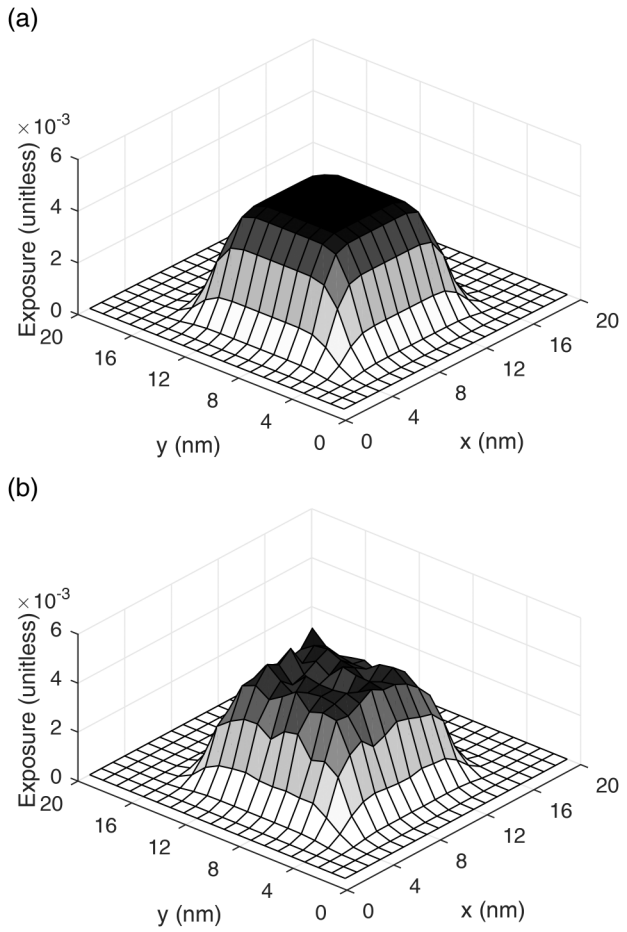

FIG. 2. (a) Deterministic transfer function for the beam aperture of size $10 \times 10\,\text{nm}^2$, and (b) same transfer function with 7% noise added.

where $TF_s(x, y, z)$ represents the stochastic transfer function, $TF_n(x, y, z)$ is the absolute fluctuation (noise) added to the transfer function, c is a random number from normal distribution $N(0, 1)$, ϵ is the percentage of noise to be added (e.g., 0.05 or 5%), and $0 < \alpha < 1$.

III. REALIZATION OF SPATIAL DOSE DISTRIBUTION

To have a sufficient spatial control of the dose distribution, the line feature of width W is partitioned into five regions along its length dimension and a dose d_i is determined for each region i where $i = 1, 2, 3, 4, 5$ (Fig. 3). In a previous study,[6] four different types of spatial dose distributions are introduced, i.e., uniform, V-type, A-type, and M-type. It is shown in another study[7] that reducing the feature width to be exposed results in a smaller CD error and LER. However, due to a relatively large beam size B and a fixed exposing interval I_{ex} in the current MPES, the optimal line-width reduction ΔW and spatial distribution of dose required for

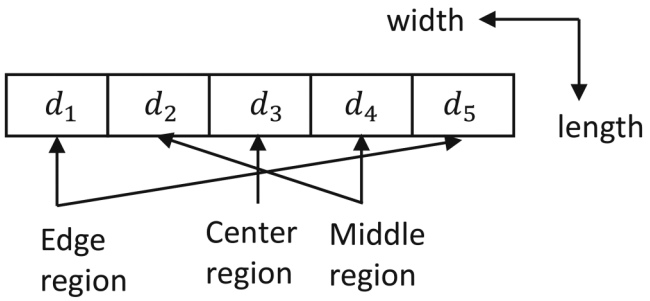

FIG. 3. Feature is partitioned into five regions such that the dose can be spatially controlled region-wise. The spatial dose distribution $\{d_i\}$ is symmetric with respect to the center region, i.e., $d_1 = d_5$ and $d_2 = d_4$.

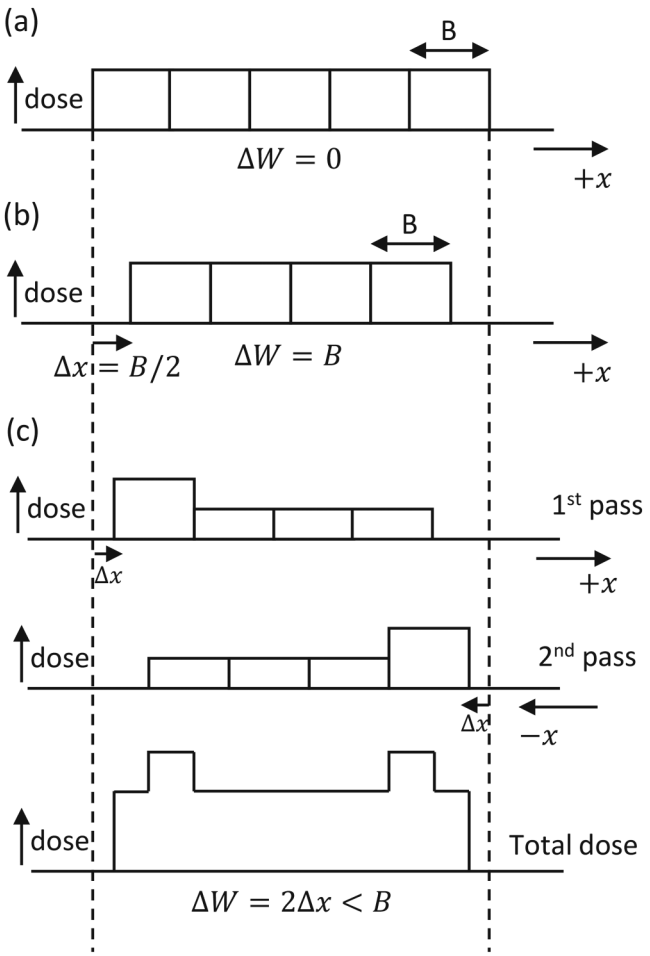

FIG. 4. Total dose is given in one pass when (a) $\Delta W = 0$ and (b) $\Delta W = B$. More than one pass is used to realize a dose distribution when (c) $0 < \Delta W < B$.

the proximity effect correction may not be achievable. Therefore, a practical method for realizing a given type of dose distribution with any ΔW is needed.

From Fig. 4, it can be seen that, when $\Delta W = nB$ where n is a non-negative integer, any type of dose distribution can be realized in one pass as the width of feature to be exposed is an integer multiple of B. But, when $\Delta W \neq nB$, the number of passes, n_p, is greater than one to realize the dose distribution as close to the target dose distribution as possible. Also, the point of exposure on the substrate for each beam needs to be shifted by the amount of $\Delta x = \frac{\Delta W}{2}$ in the direction of substrate as illustrated in Fig. 4(c). In such cases, there can be some regions where the given dose is higher than the target dose due to the overlap of exposed regions [Fig. 4(c)]. Hence, the dose to be given to each region in each pass needs to be determined such that the overlap and dose deviation are minimized.

Another important issue to consider is the utilization of beams in an MPES. Utilization U is defined as the average fraction of time the beams are on with respect to the total exposing time. Suppose that five beams are exposing a feature of five pixels. Each beam is deflected five times exposing a pixel. If all the beams are on in all 25 shots (5 shots per beam), $U = 100\%$. The utilization may also be computed as the ratio of the average dose per pixel to the maximum dose given to a pixel.

The realization of uniform, V-type, A-type, and M-type dose distributions for $0 < \Delta W < B$ is described in the following. A dose distribution with the linewidth reduction of $\Delta W + nB$ can be realized in the same way as for the linewidth reduction of ΔW. It is assumed that the feature is divided into five regions where each region consists of a pixel of size B and five beams are used to expose the feature. The beam size of $B = 10$nm and the beam interval of $I_{bx} = 4B$ are considered. In a *step*, a beam gives a unit dose of d to a pixel. During the exposing process, each beam follows a pixel being deflected five times, to give a total dose of $D = 5d$ to the pixel through a cycle of 5 steps.

A. Uniform dose distribution

In Fig. 5, the realization of uniform dose distribution is illustrated with different linewidth reductions, ΔW. When $\Delta W = nB$, a uniform dose distribution can be achieved in one pass [Fig. 5(a)]. On the other hand, when $\Delta W \neq nB$, a (completely) uniform dose distribution cannot be achieved though the deviation from the uniform distribution may be minimized through multiple passes. In Figs. 5(b)–5(d), the dose to be given to each region in each pass is shown to realize a uniform dose distribution for $0 < \Delta W < B$. The doses in the gray areas in Fig. 5 are higher than the target (desired) dose due to the overlap of exposed regions over multiple passes. To avoid too high a dose in the gray areas, the final dose in the edge regions may be made smaller than that in the center and middle regions. In Fig. 6, the ideal and realized dose distributions are illustrated. The utilization U with $\Delta W \neq nB$ is smaller than that with $\Delta W = nB$ as shown in Fig. 5. This is because some beams remain off when a region gets no dose or a smaller dose than other regions in different passes.

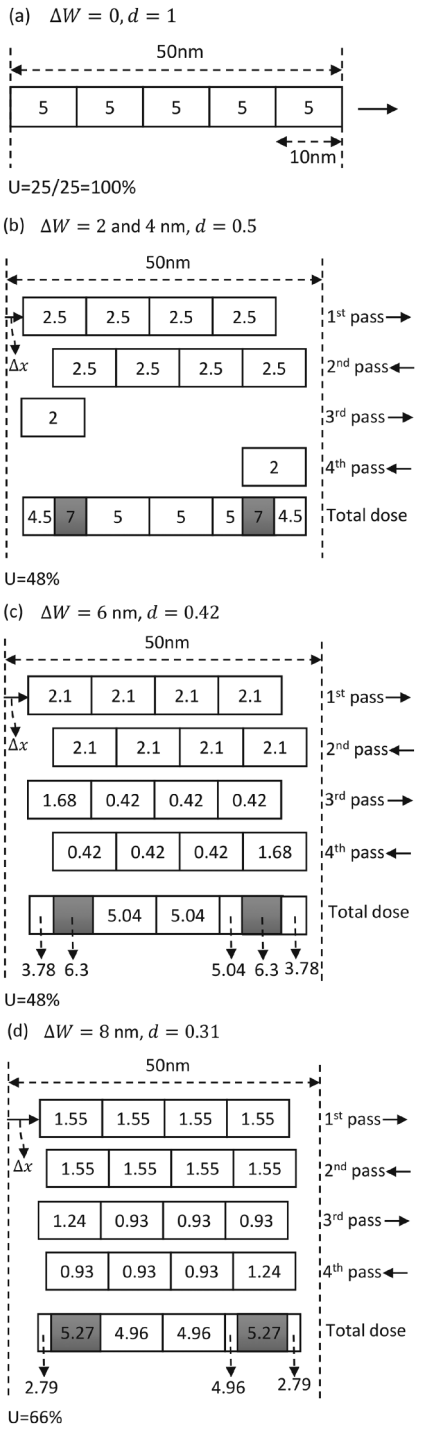

FIG. 5. Realization of uniform dose distribution in multiple passes for (a) $\Delta W = 0$ nm and $n_p = 1$, (b) $\Delta W = 2$ and 4 nm, and $n_p = 4$, (c) $\Delta W = 6$ nm and $n_p = 4$, and (d) $\Delta W = 8$ nm and $n_p = 4$. The gray areas represent higher dose than the target dose due to the overlap of exposed regions in multiple passes.

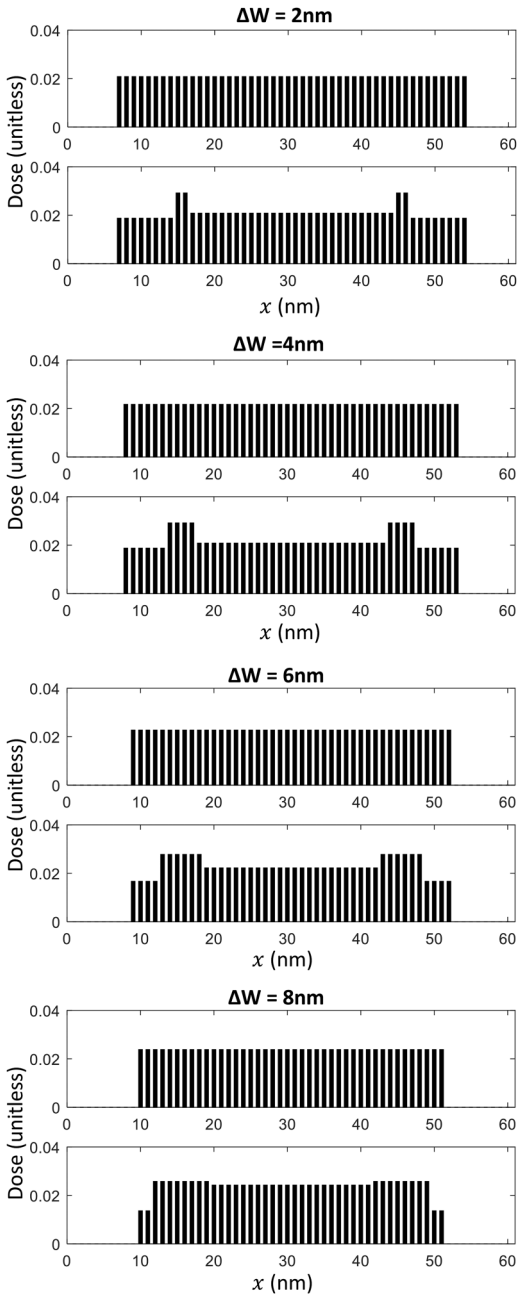

FIG. 6. Ideal (top) and realized (bottom) uniform dose distributions for each of $\Delta W = 2, 4, 6,$ and 8 nm.

B. V-type dose distribution

The realization of V-type dose distribution with varying ΔW is illustrated in Fig. 7. The number of passes may vary depending on the spatial-dose-distribution ratio and d. In general, more passes are needed with $\Delta W \neq nB$ than with $\Delta W = nB$. The overlapped

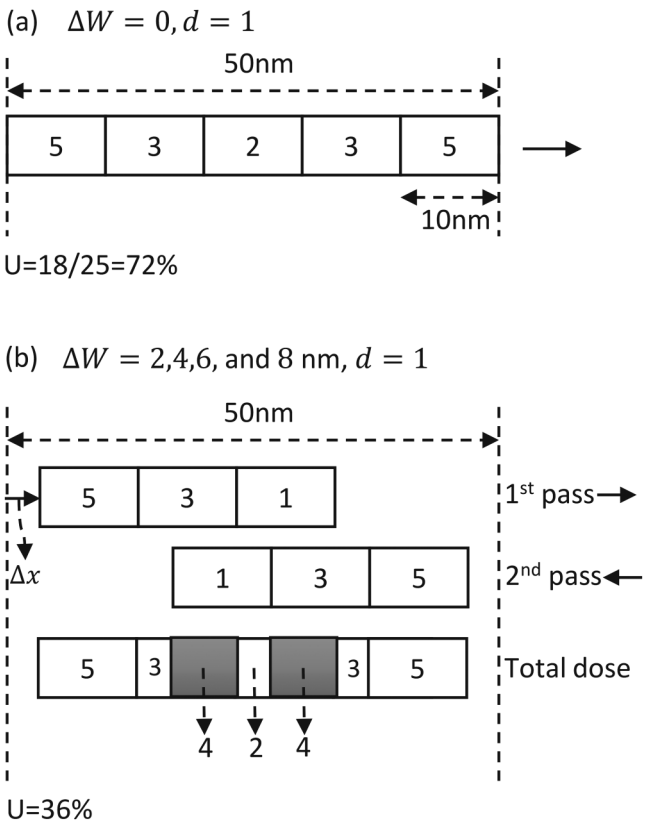

FIG. 7. Realization of V-type dose distribution in multiple passes with a spatial-dose-distribution ratio of 5:3:2:3:5 for (a) $\Delta W = 0$ nm and $n_p = 1$, and (b) $\Delta W = 2$, 4, 6 and 8 nm, and $n_p = 2$. The gray areas represent higher dose than the target dose due to the overlap of exposed regions in multiple passes.

(gray) areas between the middle and center regions when $\Delta W \neq nB$ cause the realized V-type dose distribution to deviate from the ideal V-shape as shown in Fig. 8. The utilization U with $\Delta W \neq nB$ is smaller than that with $\Delta W = nB$, as more beams are turned off in more passes when $\Delta W \neq nB$. Also, U for the V-type dose distribution tends to be lower than that for the uniform dose distribution (see Fig. 7).

C. A-type dose distribution

The realization of A-type dose distribution with varying ΔW is illustrated in Fig. 9. Because of the overlapped (gray) areas between the middle and center regions, the realized A-type dose distribution is smoother than the ideal A-shape as shown in Fig. 10. Also, the utilization U for the A-type may change depending on the spatial-dose-distribution ratio which also determines the number of passes required. U tends to be lower when the dose in the center region is higher. This is because the number of steps increases to provide the high dose in the center region, but the beams remain off most of the time while exposing other regions.

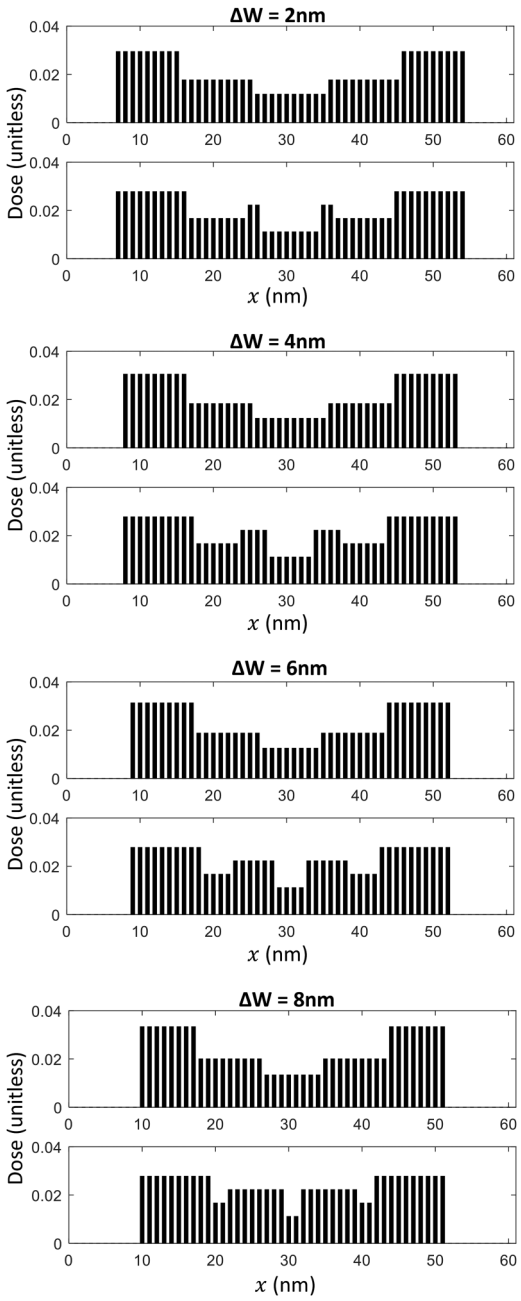

FIG. 8. Ideal (top) and realized (bottom) V-type dose distributions for each of $\Delta W = 2$, 4, 6, and 8 nm.

D. M-type dose distribution

The realization of M-type dose distribution with varying ΔW is demonstrated in Fig. 11. There are overlapped (gray) areas between the edge, middle, and center regions (Fig. 11), which results in a blurred transition between the regions as can be seen in Fig. 12, where the ideal and realized dose distributions are compared with varying ΔW. In general, the utilization U with $\Delta W \neq nB$ is smaller than that with $\Delta W = nB$, since more passes are required when $\Delta W \neq nB$ where more beams stay off.

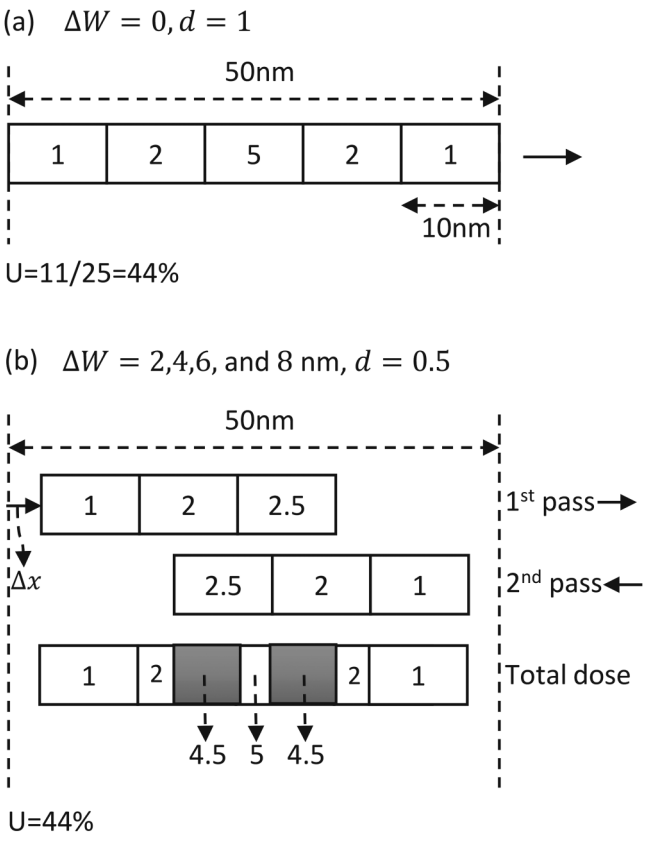

FIG. 9. Realization of A-type dose distribution in multiple passes with a spatial-dose-distribution ratio of 1:2:5:2:1 for (a) $\Delta W = 0$ nm and $n_p = 1$, and (b) $\Delta W = 2$, 4, 6 and 8 nm, and $n_p = 2$. The gray areas represent higher dose than the target dose due to the overlap of exposed regions in multiple passes.

IV. MINIMIZATION OF CD ERROR AND LER

In this section, the realization of the shape + dose correction method is described under the constraints of the MPES to minimize the CD error and LER.

A. Cost function

In a previous study,[7] it was observed that the CD error and LER stay low when the edge of the developed feature is outside the exposed area. This is because the exposure level quickly drops from the exposed area (inside the feature) to the unexposed area (outside the feature) and the absolute variation of exposure is smaller in the unexposed area. It is possible that the optimal ΔW for the minimal CD error is not the same as that for the minimal LER. Also, the required total dose may increase significantly while reducing the

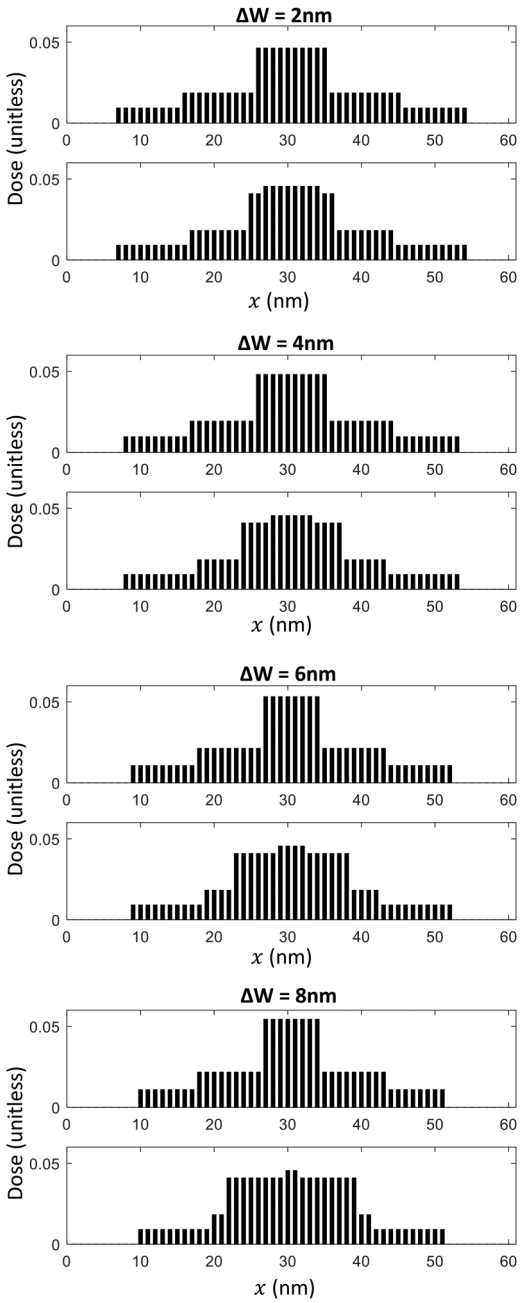

FIG. 10. Ideal (top) and realized (bottom) A-type dose distributions for each of $\Delta W = 2, 4, 6,$ and 8 nm.

linewidth to be exposed. Therefore, the cost function, C, consisting of the CD error, LER, and total dose is considered,

$$C = \alpha Error_{CD} + \beta LER + \gamma Dose_{total}, \quad (4)$$

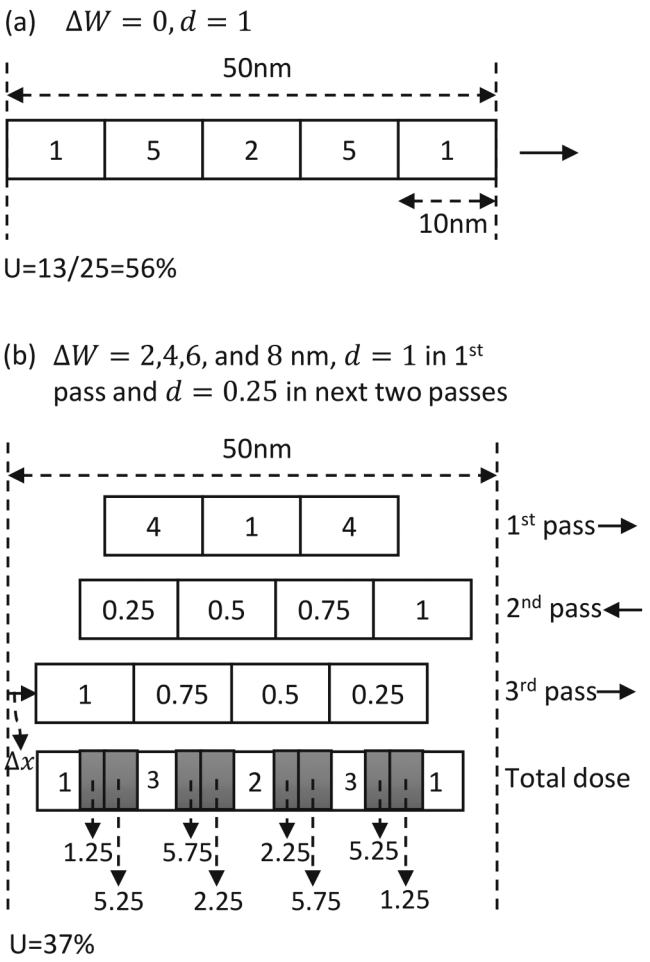

FIG. 11. Realization of M-type dose distribution in multiple passes with a spatial-dose-distribution ratio of 1:5:2:5:1 for (a) $\Delta W = 0$ nm and $n_p = 1$, and (b) $\Delta W = 2$, 4, 6 and 8 nm, and $n_p = 3$. The gray areas represent higher dose than the target dose due to the overlap of exposed regions in multiple passes.

where α, β, and γ are the weights given to $Error_{CD}$, LER, and $Dose_{total}$, respectively.

The $Error_{CD}$ is measured as the absolute difference between the target and actual edge locations, averaged over the top, middle, and bottom layers. The LER is quantified as the standard deviation of edge location. The $Dose_{total}$ is the integration of area dose over the feature width.

B. Shape + dose correction

The optimal linewidth reduction and the dose to be given to each region for different types of dose distributions are determined through an iterative procedure such that the cost function is minimized. The correction procedure does not allow the dose of a region to exceed a certain value to avoid too low a utilization. Also, it exploits the fact that the cost function shows a bitonic behavior

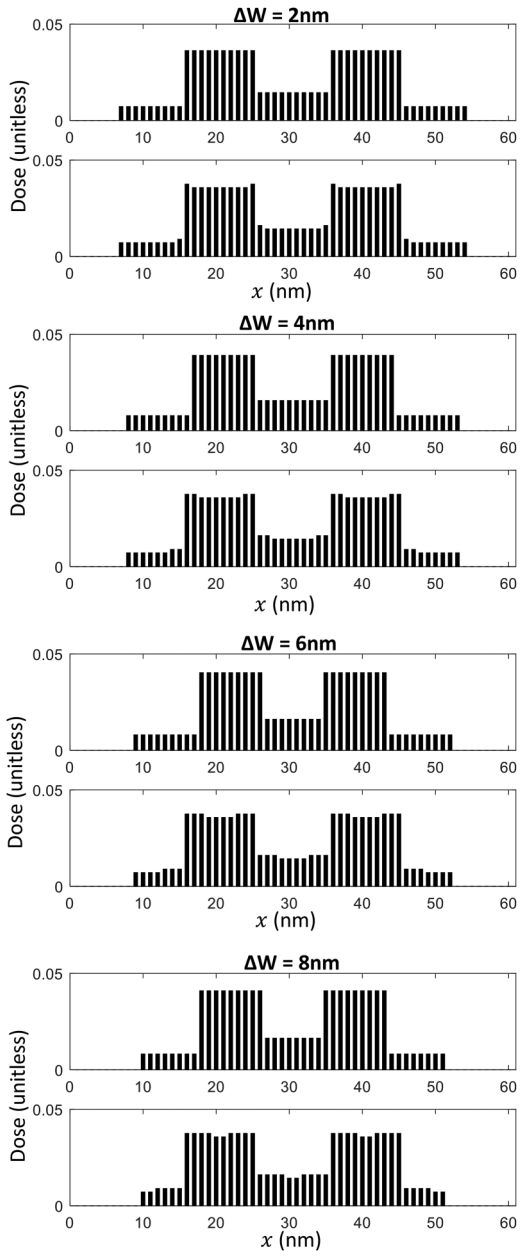

FIG. 12. Ideal (top) and realized (bottom) M-type dose distributions for each of $\Delta W = 2, 4, 6,$ and 8 nm.

with respect to ΔW. The following notations are used in the description of the procedure.

- The minimum value of cost function.
- The minimum value of cost function for a ΔW.
- The initial value of cost function.
- The maximum dose allowed in a region.
- The amount of adjustment for d_i. $\Delta d_i = d_i \times x$ where $0 < x < 1$.
- The optimal linewidth reduction
- The optimal spatial dose distribution.
- Initialized to {3,2,1,2,3} for V-type, {1,2,3,2,1} for A-type, and {1,2,1,2,1} for M-type.

The iterative correction procedure for a given type of dose distribution is described below where k is the iteration index, and its flow chart is also provided in Fig. 13. It consists of two nested loops where different amounts of width reduction are considered through the outer loop while the spatial dose distribution is optimized for a given feature width in the inner loop. It is assumed that the minimum possible reduction of width is 2 nm, i.e., 1 nm on each side of feature.

(1) $\Delta W \leftarrow 0$, $C_{min} \leftarrow$ a large value, $C_{min,\Delta W} \leftarrow$ a large value, and $C_0 \leftarrow$ a large value.
(2) Initialize $\{d_i\}$ according to the type of dose distribution and x.
(3) Obtain the realizable dose distribution given ΔW and $\{d_i | i = 1, 2, 3, 4, 5\}$. Refer to Sec. III.
(4) Evaluate the cost function, C_k.
(5) If $C_k < C_{min}$,

$$C_{min} \leftarrow C_k, \Delta W_{opt} \leftarrow \Delta W \text{ and } \{d_{i,opt}\} \leftarrow \{d_i\}.$$

(6) If $| C_k - C_{k-1} | <$ *tolerance*, go to step 10.
(7) If $C_{k-1} - C_{k-1} \times y < C_k < C_{k-1}$ where $0 < y < 1$, i.e., the improvement in C is too small,

$$x \leftarrow s_1 x \ (s_1 > 1).$$

(8) If $C_k > C_{k-1} + C_{k-1} \times y$,

$$x \leftarrow s_2 x \ (0 < s_2 < 1).$$

(9) $d_i \leftarrow d_i \pm \Delta d_i$ such that $0 < d_i \pm \Delta d_i < d_{max}$ and the dose distribution type is maintained, and go to step 3.
(10) If $C_{min} < C_{min,\Delta W}$,

$$C_{min,\Delta W} \leftarrow C_{min}, \Delta W \leftarrow \Delta W + 2 \text{ nm}, \text{ and go to step 2.}$$

(11) Output ΔW_{opt} and $\{d_{i,opt}\}$.

In step 9, the dose d_i is adjusted maintaining the relationship among region doses for the given type of dose distribution, i.e., $d_1 > d_2 > d_3$ for V-type, $d_1 < d_2 < d_3$ for A-type, and $d_1 < d_3 < d_2$ for M-type. With any type of dose distribution, if $d_i \pm \Delta d_i$ is greater than d_{max} or does not maintain the relationship (among region doses), the adjustment is attempted in the adjacent region or Δd_i is adjusted by reducing the parameter x. Figures 14–16 illustrate for different types of dose distribution how a region is selected and the dose adjustment in the region is determined. With the V-type dose distribution, there can be an inner CD error shown in Fig. 14(a) due to a low dose in the center regions. In this case, the dose in the center region is increased to remove the inner CD error. Also, with the V-type, the top layer of resist develops earlier than the bottom layer within the edge regions resulting in an overcut sidewall as shown in Fig. 14(b). This problem can be alleviated by lowering the

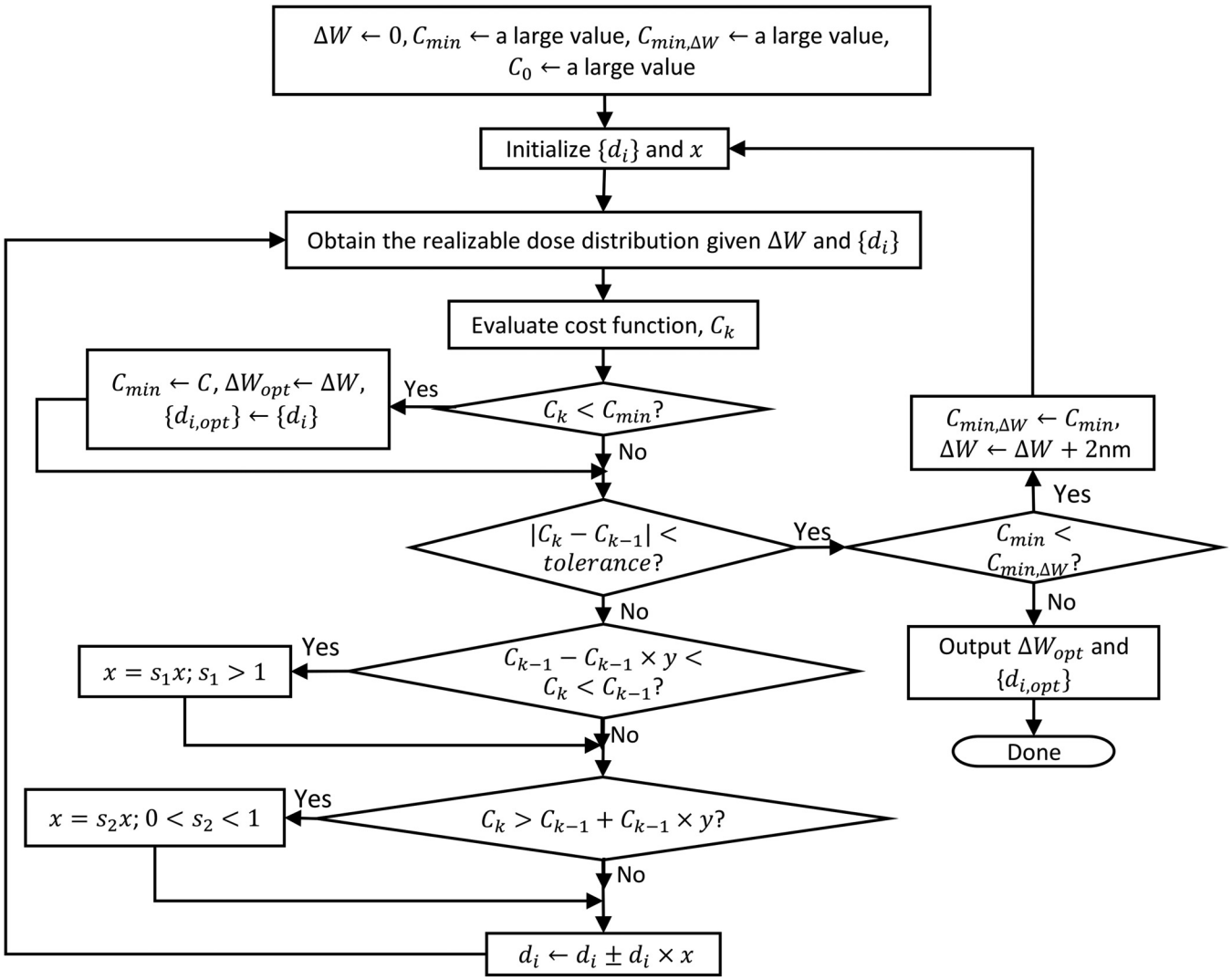

FIG. 13. Flow chart of the shape + dose correction method where k is the iteration index, and $0 < x, y < 1$.

dose in the edge regions, which reduces the top-layer CD error more than it reduces the bottom-layer CD error. In this way, the resist profiles are more balanced in the CD error among layers.

The CD in the top layer can be smaller than the target CD in the case of A-type dose distribution [Fig. 15(a)] due to a low dose in the edge regions. In such a case, the dose in the edge regions is increased to match the top-layer CD to the target CD. Also, if the CD error in the top layer is larger than that in the bottom layer with the A-type [Fig. 15(b)], the dose in the center region is increased so that the resist development in the bottom layer can catch up with that in the top layer.

An inner CD error may occur also in the case of M-type dose distribution as illustrated in Fig. 16(a), which is eliminated by increasing the dose in the center region. Also, if the CD error in the bottom layer is larger than that in the top layer with the M-type [Fig. 16(b)], the dose in the center region is increased to match the resist development in the bottom layer to that in the top layer.

V. RESULTS AND DISCUSSION

The effectiveness of the shape + dose correction algorithm under the constraints of the MPES has been analyzed for different types of dose distributions through simulation. The TF is modeled based on the 3D point spread function (PSF) generated using a Monte Carlo simulation program CASINO (Ref. 13) for the substrate system of 100 nm PMMA on Si, the beam energy of 50 keV, and the beam diameter of 6 nm. The total exposure and forward

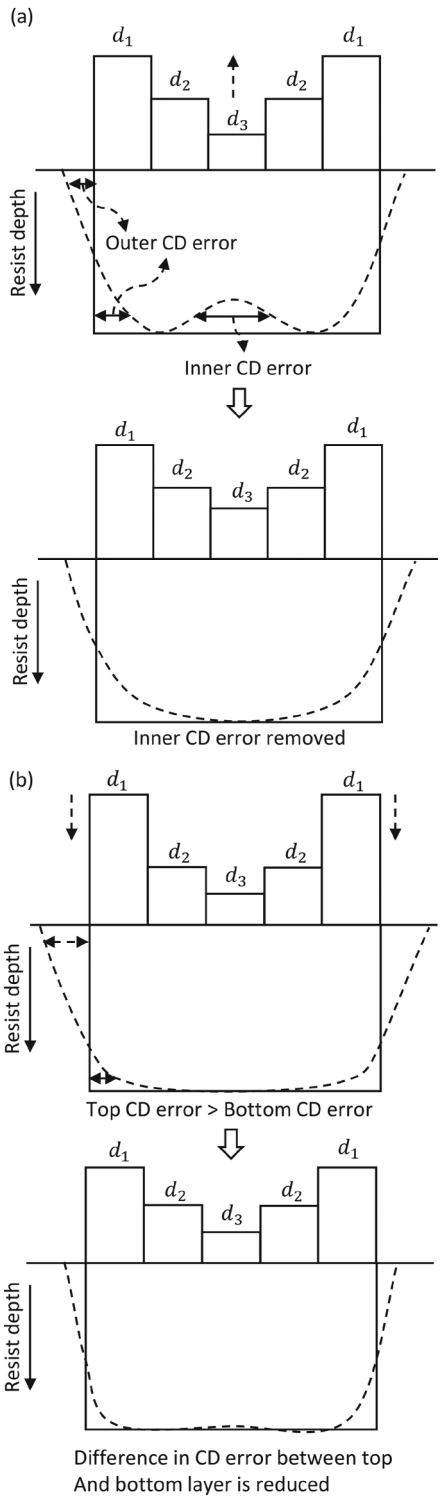

FIG. 14. Dose adjustment in the case of V-type dose distribution guided by the cross section of the resist profile.

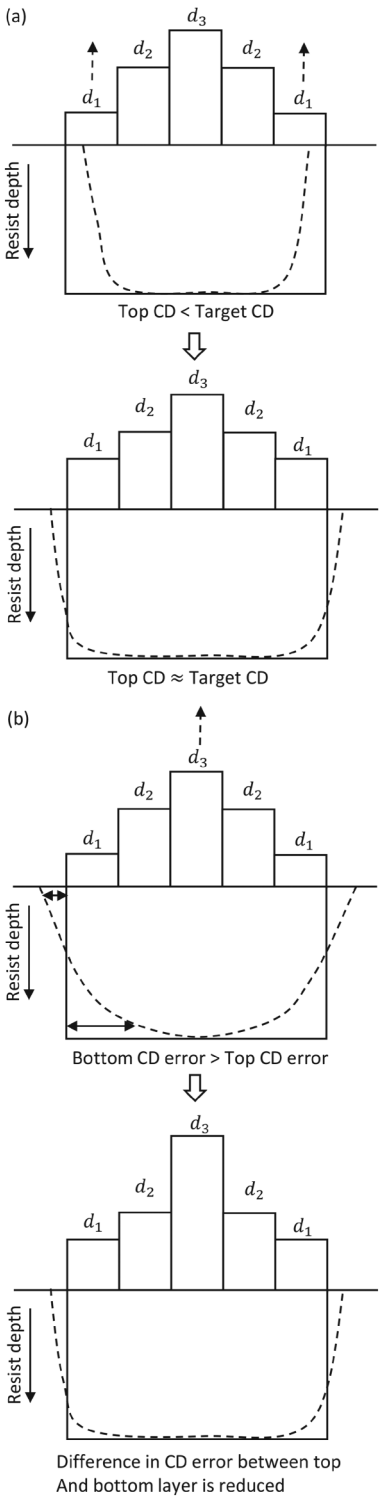

FIG. 15. Dose adjustment in the case of A-type dose distribution guided by the cross section of the resist profile.

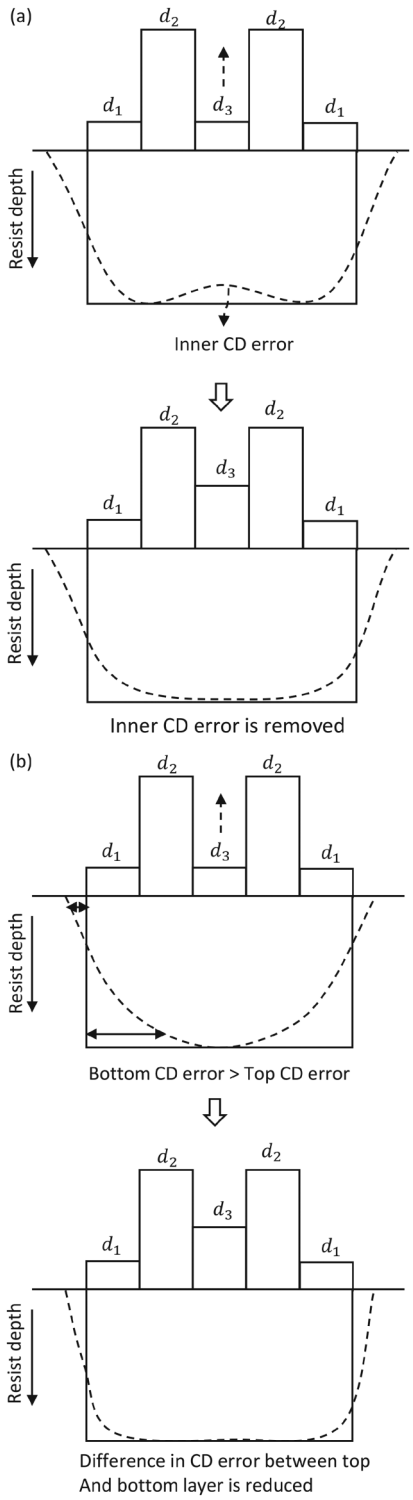

FIG. 16. Dose adjustment in the case of M-type dose distribution guided by the cross section of the resist profile.

scattering range (the standard deviation of Gaussian) are extracted from the PSF for each of the five resist layers. The ratios of the total energy and forward scattering range among the five resist layers are referred to in setting the total exposure and σ_t of the Gaussian function used to generate the TF of each layer.

The 3D exposure distribution in the resist is computed at the resolution I_{sm}, referred to as simulation interval, which is set to $\frac{1}{2}$ nm. The developing-rate distribution is derived from the exposure distribution and then the remaining resist profile is obtained through a fast path-based resist-development simulation.[14] The development simulation continues until the feature is fully developed to the bottom layer of resist. From the resist profile, the CD and LER are measured. The middle 80% segment of the developed feature along the length dimension is used in the computation of the CD and LER to exclude the edge effect (rounding at corners). The CD and LER in each case are averaged over five simulations.

Two different widths of a single-line are considered for performance analysis, i.e., 50 and 150 nm, and the length of the line is fixed at 300 nm. Each row of pixels is exposed by five beams with the beam size of 10 nm. Both sharp and broad TFs are considered, i.e., $\sigma_t = 1$ and 4 nm. The line features are corrected with four types of dose distributions, i.e., uniform, V-type, M-type, and A-type minimizing the CD error and LER at the top, middle, and bottom layers. The values of α, β, and γ in the cost function are selected to be 1, 0, and 0.2, respectively. β is set to 0 since the effect of the LER is not significant in any type of dose distribution as long as $\Delta W > 0$. As the main objective is to minimize the CD error, the weight of the CD error is five times larger than that of the total dose. In the optimization procedure, $x = 0.5$ initially, $s_1 = 2$, $s_2 = 0.5$, $y = 0.01$, and *tolerance* $= 0.005$.

The average CD error, required total dose, and LER obtained with ΔW varied are provided in Figs. 17 and 18 for the feature width of 50 nm. From the figures, it is seen that as ΔW increases, the CD error decreases up to a certain ΔW and then starts to increase. For a larger ΔW, the resist development in the bottom layer is more likely to catch up the resist development in the top layer and the resist profile achieves a more vertical sidewall. However, when ΔW is too large, the resist development in any layer cannot reach the target edge location unless a significantly high dose is given to the feature. For this reason, the CD error starts to increase after a certain ΔW. The required total dose increases exponentially with ΔW in order to develop the feature outside the exposed area. The LER decreases with the increase in ΔW, since the absolute variation of exposure is smaller in the unexposed area. The similar trends are observed in the results for the feature width of 150 nm.

These results show that it is possible to achieve the minimal CD error and very small LER with an acceptable dose level by the shape + dose correction which utilizes the spatial dose distribution realizable on an MPES.

In Tables I and III, the optimal ΔW and spatial-dose-distribution ratio obtained by minimizing only the average CD error ($\alpha = 1, \beta = 0,$ and $\gamma = 0$) with different types of dose distributions are provided for the feature width of 50 nm, while in Tables II and IV, those obtained by minimizing the cost function ($\alpha = 1, \beta = 0,$ and $\gamma = 0.2$). First, in none of the cases considered, the optimal ΔW is an integer multiple of beam size, B. This well demonstrates that a spatial dose control for the cases

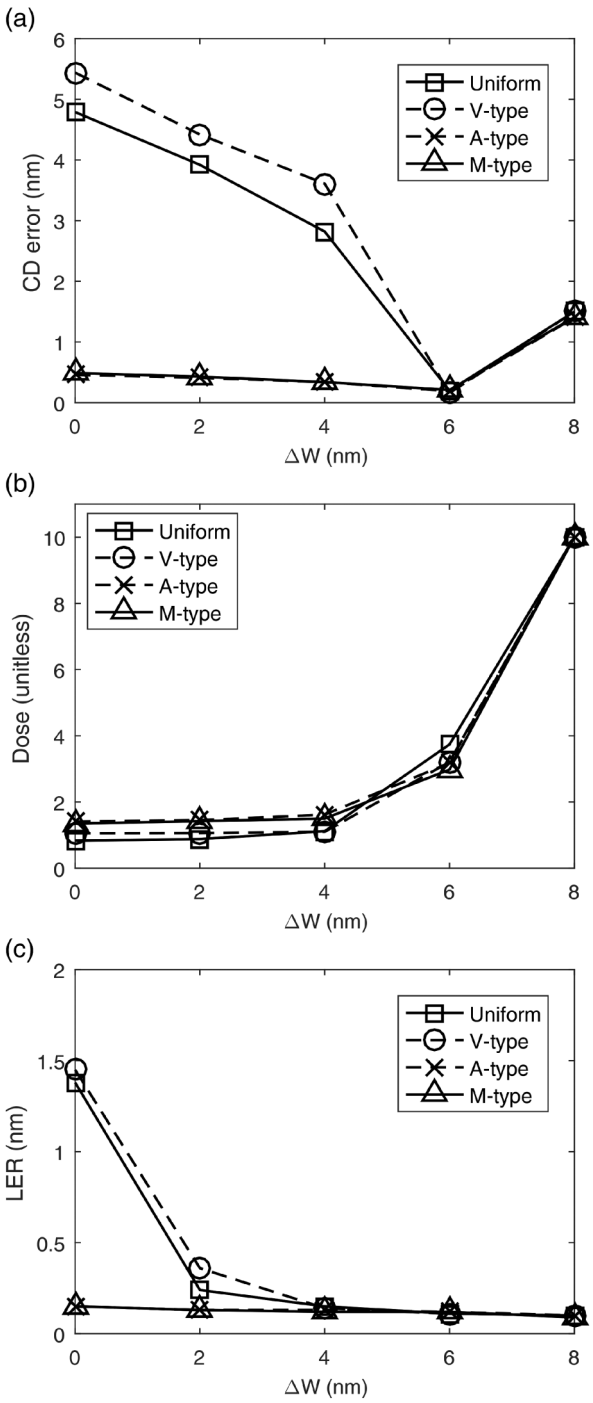

FIG. 17. (a) Average CD error over the top, middle, and bottom layers of resist, (b) total dose required, and (c) LER at the middle layer are plotted with respect to the linewidth reduction ΔW for $\sigma_t = 1$ nm where feature size: $50 \times 300\,\text{nm}^2$, beam size: $10 \times 10\,\text{nm}^2$, beam interval: 40 nm, resist thickness: 100 nm. For each ΔW, the optimal spatial-dose-distribution ratio is determined using the iterative procedure described in Sec. IV.

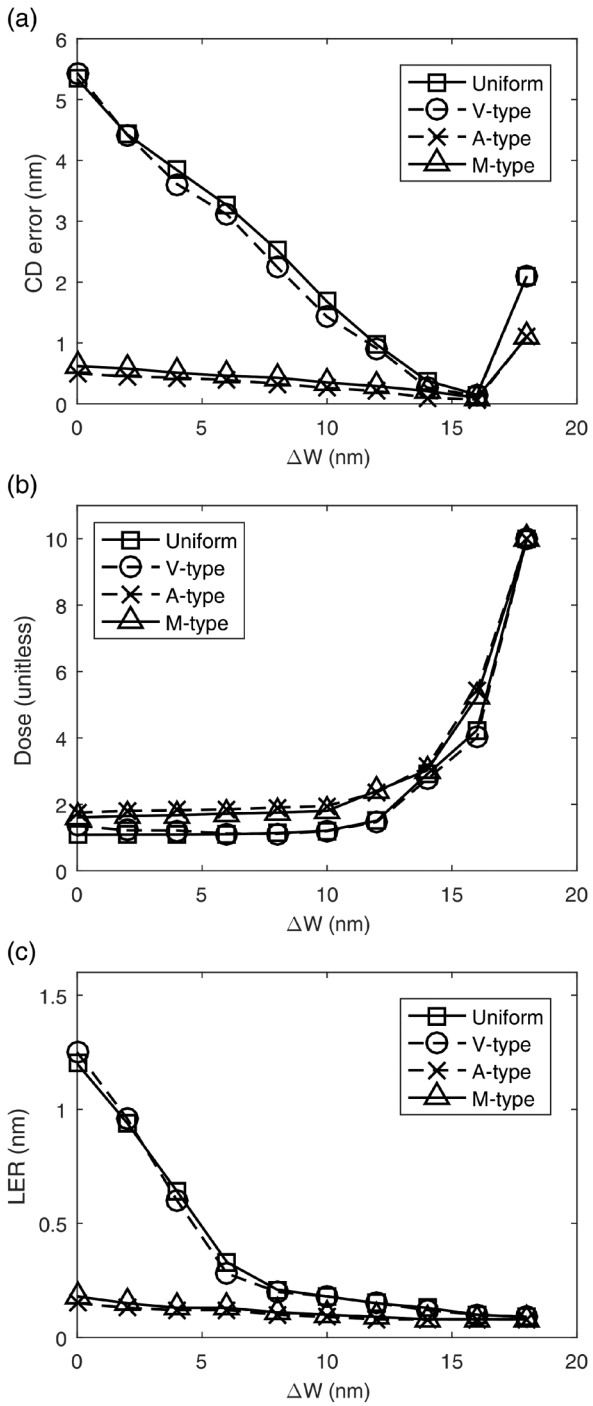

FIG. 18. (a) Average CD error over the top, middle, and bottom layers of resist, (b) total dose required, and (c) LER at the middle layer are plotted with respect to the linewidth reduction ΔW for $\sigma_t = 4$ nm where feature size: $50 \times 300\,\text{nm}^2$, beam size: $10 \times 10\,\text{nm}^2$, beam interval: 40 nm, resist thickness: 100 nm. For each ΔW, the optimal spatial-dose-distribution ratio is determined using the iterative procedure described in Sec. IV.

TABLE I. Optimal ΔW and spatial-dose-distribution ratio obtained by minimizing only the average CD error for uniform, V-type, A-type, and M-type dose distribution. $W = 50$ nm, $\sigma_t = 4$ nm.

Type	Spatial-dose-distribution ratio	Optimal ΔW (nm)	CD error (nm)	Dose (unitless)
Uniform	1:1:1:1:1	16	0.15	4.23
V	1.17:1.06:1:1.06:1.17	16	0.13	4.01
A	1:2:3.15:2:1	16	0.06	5.48
M	1:3.9:2:3.9:1	16	0.11	5.15

TABLE II. Optimal ΔW and spatial-dose-distribution ratio obtained by minimizing the cost function for uniform, V-type, A-type, and M-type dose distribution. $W = 50$ nm, $\sigma_t = 4$ nm.

Type	Spatial-dose-distribution ratio	Optimal ΔW (nm)	CD error (nm)	Dose (unitless)
Uniform	1:1:1:1:1	14	0.30	3.11
V	4.5:2:1:2:4.5	14	0.24	2.99
A	1:2:5.4:2:1	10	0.22	2.15
M	1:7.5:2:7.5:1	10	0.20	2.26

TABLE III. Optimal ΔW and spatial-dose-distribution ratio obtained by minimizing only the average CD error for uniform, V-type, A-type, and M-type dose distribution. $W = 50$ nm, $\sigma_t = 1$ nm.

Type	Spatial-dose-distribution ratio	Optimal ΔW (nm)	CD error (nm)	Dose (unitless)
Uniform	1:1:1:1:1	6	0.20	3.74
V	1.21:1.16:1:1.16:1.21	6	0.15	3.19
A	1:2:4.49:2:1	6	0.18	3.21
M	1:6.01:2:6.01:1	6	0.20	2.98

TABLE IV. Optimal ΔW and spatial-dose-distribution ratio obtained by minimizing the cost function for uniform, V-type, A-type, and M-type dose distribution. $W = 50$ nm, $\sigma_t = 1$ nm.

Type	Spatial-dose-distribution ratio	Optimal ΔW (nm)	CD error (nm)	Dose (unitless)
Uniform	1:1:1:1:1	6	0.18	3.84
V	1.21:1.16:1:1.16:1.21	6	0.15	3.24
A	1:2:5.06:2:1	4	0.30	1.74
M	1:6.75:2:6.75:1	4	0.32	1.69

when $\Delta W \neq nB$ considering the constraints of the MPES is necessary to obtain the optimal correction results. Second, it is seen that the CD error achieved by the shape + dose correction method is very small in all cases. That is, the spatial dose distributions realized on an MPES are effective though they deviate from the ideal distributions. Third, the nonuniform dose distributions give better results in most of the cases than the uniform dose distribution, which illustrates the importance of realizing nonuniform dose distributions with varying ΔW. Fourth, the optimal ΔW and spatial-dose-distribution ratios are different between without (i.e., CD error only) and with considering the cost function in most cases for both σ_t of 1 nm and 4 nm. That is, minimizing the CD error only is not necessarily optimal when the total dose also needs to be taken into account. The required total dose can be made smaller (as seen in Tables II and IV) by increasing its weight in the cost function such that the average CD error still remains relatively small.

VI. SUMMARY

MPES systems have some constraints compared to the single-beam systems, e.g., a relatively large beam size, a fixed exposing interval, and the same deflection angle for all beams. The shape + dose correction method previously introduced for the single-beam systems requires a reduction of feature width and spatial control of dose. The direct application of this correction method to the MPES system may lead to nonoptimal correction results unless the optimal linewidth reduction (ΔW) is an integer multiple of the beam size. In this study, a practical method of realizing four types of dose distributions, i.e., uniform, V-type, A-type, and M-type, with varying linewidth reduction (ΔW) under the constraints of the MPES has been developed, and is applicable to any spatial-dose-distribution ratio. Also, a shape + dose correction procedure which uses the spatial dose distribution (with a width reduction) realizable on an MPES has been designed and implemented. Through an extensive simulation, it has been shown that the shape + dose correction procedure can optimally reduce the CD error and LER while maintaining a relatively low total dose. In most cases, the optimal ΔW is not an integer multiple of the beam size and the nonuniform dose distributions perform better than the uniform dose distribution. These results clearly show that it is essential to have practical methods to realize various spatial dose distributions with any ΔW on an MPES. Therefore, the method of spatial-dose realization and the procedure of shape + dose correction developed in this study may be referred to in correcting the proximity effect for massively parallel e-beam systems.

ACKNOWLEDGMENTS

This work was supported in part by a research grant from Samsung Electronics Co., Ltd.

REFERENCES

[1]M. Osawa, K. Ogino, H. Hoshino, Y. Machida, and H. Arimoto, J. Vac. Sci. Technol. B **22**, 2923 (2004).
[2]R. Murali, D. K. Brown, K. P. Martin, and J. D. Meindl, J. Vac. Sci. Technol. B **24**, 2936 (2006).

[3]S.-Y. Lee and K. Anbumony, J. Vac. Sci. Technol. B **25**, 2008 (2007).
[4]K. Ogino, H. Hoshino, and Y. Machida, J. Vac. Sci. Technol. B **26**, 2032 (2008).
[5]N. Unal, D. Mahalu, O. Raslin, D. Ritter, C. Sambale, and U. Hofmann, Microelectron. Eng. **87**, 940 (2010).
[6]Q. Dai, S.-Y. Lee, S.-H. Lee, B.-G. Kim, and H.-K. Cho, J. Vac. Sci. Technol. B **30**, 06F307 (2012).
[7]X. Zhao, S.-Y. Lee, J. Choi, S.-H. Lee, I.-K. Shin, C.-U. Jeon, B.-G. Kim, and H.-K. Cho, Microelectron. Eng. **133**, 78 (2015).
[8]C. Klein, H. Loeschner, and E. Platzgummer, J. Micro/Nanolithogr. MEMS MOEMS **11**, 031402 (2012).
[9]H. Matsumoto, H. Inoue, H. Yamashita, T. Tamura, and K. Ohtoshi, J. Micro/Nanolithogr. MEMS MOEMS **17**, 031205 (2018).
[10]A. Fay *et al.*, Proc. SPIE **9777**, 977714 (2016).
[11]M. N. Hasan, S.-Y. Lee, B.-S. Ahn, J. Choi, S.-B. Kim, and C.-U. Jeon, J. Vac. Sci. Technol. B **37**, 061609 (2020).
[12]H. Ji, S.-Y. Lee, J. Choi, S.-B. Kim, I.-K. Shin, and C.-U. Jeon, J. Vac. Sci. Technol. B **35**, 06G503 (2017).
[13]D. Drouin, A. R. Couture, D. Joly, X. Tastet, V. Aimez, and R. Gauvin, Scanning **29**, 92 (2007).
[14]Q. Dai, R. Guo, S.-Y. Lee, J. Choi, S.-H. Lee, I.-K. Shin, and C.-U. Jeon, Microelectron. Eng. **127**, 86 (2014).